Understanding of selective oxidation of Fe-Mn binary alloys during continuous annealing through X-ray photoelectron spectroscopy

L. Gong, David Alamarguy, N. Ruscassier, Paul Haghi-Ashtiani, M.-L. Giorgi

Research article

Understanding of selective oxidation of Fe-Mn binary alloys during continuous annealing through X-ray photoelectron spectroscopy

L. Gong [1,2 *], D. Alamarguy [3], N. Ruscassier [1], P. Haghi-Ashtiani [4], M.-L. Giorgi [1]

[1] LGPM, CentraleSupélec, Université Paris Saclay, 3 rue Joliot-Curie, 91192 Gif-sur-Yvette cedex, France,

[2] Key Laboratory of Advanced Materials of Ministry of Education, School of Materials Science and Engineering, Tsinghua University, Beijing 100084, China,

[3] GeePS, CentraleSupélec, Université Paris Saclay, 11 rue Joliot-Curie, 91192 Gif-sur-Yvette cedex, France,

[4] MSSMat, CNRS, CentraleSupélec, Université Paris Saclay, 3 rue Joliot-Curie, 91192 Gif-sur-Yvette cedex, France

[*] Corresponding author.

E-mail address: gongli@mail.tsinghua.edu.cn (L. Gong)

ARTICLE INFO

Article history:

Received 23 August 2022

Received in revised form 16 October 2022

Accepted 16 October 2022

Available online

Abstract

Selective oxidation of Fe-Mn alloys was characterizied through X-ray photoelectron spectroscopy and scanning/transmission electron microscopy during industrial continuous annealing (in an atmosphere of N_2-5 vol.% H_2 with traces of water at 800 °C). After annealing, only MnO oxides are formed on and below the surface and few iron oxides appear on the top surface due to oxidation of ambient air or the formation of FeO-MnO solid solutions. Mn concentration profiles exhibit typical selective oxidation and show similar features. Mn concentration first increases to a peak value at a depth of 5−10 nm from surface, and then decreases to the minimum at the oxidation front, following with a floating up and down to bulk composition. According to XPS spectra and Mn concentration profiles as a function of depth, the annealed alloy surfaces can be divided into

four zones: ambient air contaminated zone, MnO enrichment zone (external and internal oxidation coexisting here), Mn depletion zone and bulk composition zone. Mn concentration reaches a minimum value at the oxidation front, whose position is deeper with annealing temperature and time increasing. The value of Mn diffusion coefficient in ferrite estimated using diffusion flux at the oxidation front is 2.9×10^{-15} m^2 s^{-1} at 800 °C, which is slightly greater than that in literature.

Keywords: selective oxidation, X-ray photoelectron spectroscopy, concentration profile, oxidation front, diffusion coefficient

1 Introduction

Alloying elements, such as manganese, silicon, aluminum and chromium, are added to steel and Fe-based alloys for desired mechanical performance. However, these alloying elements show complicated oxidation behavior in steel during annealing at high temperature [1-6]. High-temperature annealing treatment is usually conducted in an atmosphere of nitrogen and hydrogen (5−15 vol.%), containing only traces of water (-40 °C dew point). The annealing conditions are reducing with respect to iron oxides, but oxidizing for alloying elements. During this process, alloying elements diffuse to the surface and react with the dissociative oxygen atoms. Oxides with various species and complex morphology are formed on or under steel surface, depending on amount of alloying elements, hydrogen content and dew point of the atmosphere and annealing temperature [2-4,7-12]. The presence of these oxides on steel surface will deteriorate the wettability of liquid zinc, and hence surface coating quality. Thus, characterizing the oxidation process during annealing and controlling the formation of oxides is to improving the surface properties of annealed products.

The selective oxidation phenomenon has been extensively studied in the context of industrial continuous annealing with conventional surface analytical methods. Scanning electron microscopy (SEM), atomic force microscopy (AFM), X-ray photoelectron spectroscopy (XPS) and glow discharge optical emission spectroscopy (GDOES) have been used for these studies. Results from literature show that reactive elements such as Mn, Si and Al diffuse from steel bulk to surface and precipitate as oxides on or below the steel surface under the industrial annealing conditions [1-4,7-12]. The in-depth concentration profiles of the alloying elements show that diffusion of Mn and Si in steel results in concentration gradients at surface and that an oxidation front at a depth that varies from 100 to 900 nm delimits the area where selective oxides precipitate [1,2,4,5,8,9,12-17].

Although several approaches have been used to study the selective oxidation of Mn in iron-based alloys in a broad manner, e.g. the nature and morphology of oxides and Mn diffusion and surface

enrichment, knowledge is desired regarding the evolution and distribution of Mn oxides and Mn concentration profiles as a function of time in context of industrial continuous annealing. This work, therefore, aims to characterize the evolution of Mn diffusion and oxide distribution as a function of time during continuous annealing and construct a detailed selective oxidation model of Fe-Mn alloys with kinetic parameters.

2 Experimental

2.1 Sample preparation

One millimeter thick cold rolled sheet was supplied by Goodfellow and its composition is shown in Table 1. Prior to the experiments, the sheet was cut into 20 mm square samples. The samples were first annealed at 950 °C for 60 min in a tubular resistance furnace (ETR 1200) with a high-purity nitrogen or helium atmosphere (Air Liquide, less than 3×10^{-4} vol.% H_2O, 2×10^{-4} vol.% O_2 and 5×10^{-5} vol.% C_nH_m), which was introduced at a flowrate of 3×10^{-5} m^3 s^{-1} at standard temperature and pressure conditions (0 °C; 100 kPa). After 60 min-annealing, the samples were cooled to room temperature at a rate of less than 1 °C s^{-1} in the furnace chamber. The recrystallized samples were mechanically polished with SiC papers to remove the iron oxides layer and mirror-polished up to 1 µm diamond suspension, resulting in an average roughness of a few nanometers. In the end, the samples were ultrasonically cleaned in a pure ethanol solution and completely dried. The obtained samples have a completely recrystallized microstructure with no iron oxides on the surface.

Table 1 Composition of the Fe-Mn alloy sheet studied (wt.%).

C	Si	Mn	P	S	N	Cu	Ni	Fe
0.0013	0.002	1.043	0.002	0.001	0.0028	0.001	0.002	Bal.

The obtained samples were then annealed in the quartz chamber of an infrared radiation furnace (Ulvac Sinku-Riko parabolic tubular furnace) under conditions comparable to those of industrial continuous annealing. The commercial gas mixture of high-purity N_2 and 5 vol.% H_2 (Air Liquide with less than 3×10^{-4} vol.% of H_2O and 2×10^{-4} vol.% of O_2) was introduced into the furnace chamber at a flowrate of 1.25×10^{-5} m^3 s^{-1} at standard temperature and pressure conditions (0 °C; 100 kPa). Two aluminum oxide moisture probes were placed at the gas inlet and outlet to measure the dew point in the furnace chamber. When the dew point in the quartz chamber was stable at -40 ± 2 °C, i.e. an oxygen partial pressure of 5.7×10^{-19} Pa at 800 °C [18], the annealing treatment was

started. The samples were first heated to 800 °C at a rate of 6 °C s^{-1} and then held at this temperature for 60, 120 and 240 s before being cooled down to room temperature. Due to low temperature in the furnace chamber, the cooling rate is so large (approximate 4.5 °C s^{-1} down to 650 °C) that acts as a quench for selective oxidation reactions. In order to study the oxidation kinetics, the annealing treatment was interrupted at various temperatures during heating process, e.g. 680, 700, 730, 750 and 800 °C. The eight temperature profiles are shown in Fig. 1.

2.2 X-ray photoelectron spectroscopy surface analysis

After annealing treatment, samples were partly covered with oxide particles, whose chemical composition and state were analyzed by XPS. XPS measurements were performed using a PHI 5000 VersaProbe spectrometer with a monochromatized Al K_α primary X-ray source (hv = 1486.6 eV) operated at 15 kV and 25 W. The diameter of the analyzed surface was approximately 200 µm (the mean ferrite grain diameter is 73 ± 39 µm after annealing in the infrared furnace). XPS spectra were recorded with a take-off angle of 45° with respect to the normal direction of the sample. High-resolution spectra of C 1s, O 1s, Fe 2p and Mn 2p core lines were collected with 23.5 eV pass energy, i.e. an energy step of 0.1 eV and time/step of 50 ms. The chemical state was analyzed from the binding energy of XPS spectra of each element. The in-depth profiles were obtained by 500 V ion sputtering for 10 min and then 2 kV ion sputtering for 70 min. The sputtering rate was estimated to be 0.93 and 9.5 nm/min for 500 V and 2 kV Ar ion beam respectively (testing on a standard sample of pure iron and eq. Fe in short), by assuming that the sputtering rate for Fe was comparable to that of Fe-Mn (1 wt.%) alloy. To precisely identify the changes in chemistry state on the very top surface, the XPS analysis for each sample was done as follows: the first XPS analysis was performed on the sample surface. Then, an ion sputtering was carried out at 500 V for 1 min to reach the depth of 0.93 nm (eq. Fe) from sample surface and the second XPS analysis was carried out there. The following 10 analyses were performed after 1 min of ion sputtering at 500 V each. The 11^{th} XPS analysis was therefore carried out at the depth of 9.3 nm (eq. Fe). Subsequently, the XPS analyses were performed every 2 min of ion sputtering at 2 kV, i.e., every 19 nm (eq. Fe) depth. Therefore, the depth of the 46^{th} XPS analysis is 674.3 nm (eq. Fe) from sample surface. A dual beam charge neutralization was used during depth profiling. The number of electrons detected in each characteristic peak is directly related to the amount of element in the sample analyzed and the chemical concentration was obtained from the intensity of XPS spectra as well as the relative sensitivity factor of each element. During XPS test, all XPS spectra were calibrated by setting the main C 1s peak position at 284.8 eV, and a Shirley-type background was utilized to remove the background from the high-resolution core-line XPS spectra.

2.3 STEM observation and EDS analysis

To compare the XPS results with lateral distribution of O, Fe and Mn in the alloys, STEM observations and Energy Dispersive Spectroscopy (EDS) analysis were conducted on the lateral side of the samples annealed at 800 °C for 60 s. A protective Pt layer with 1 µm thick was first deposited on the sample surface to prevent damage during lamellae preparation and a Focused Ion Beam Scanning Electron Microscope (FIB-FEI Helios NanoLab 660) was used to extract thin foils in the annealed samples. FIB foils was 15 µm long and 5 µm wide and their thickness was 80–100 nm. FIB foils were then observed using a Scanning/Transmission Electron Microscope (TEM/STEM-FEI Titan3 G2 60-300). The oxides' composition was analyzed by EDS in TEM/STEM.

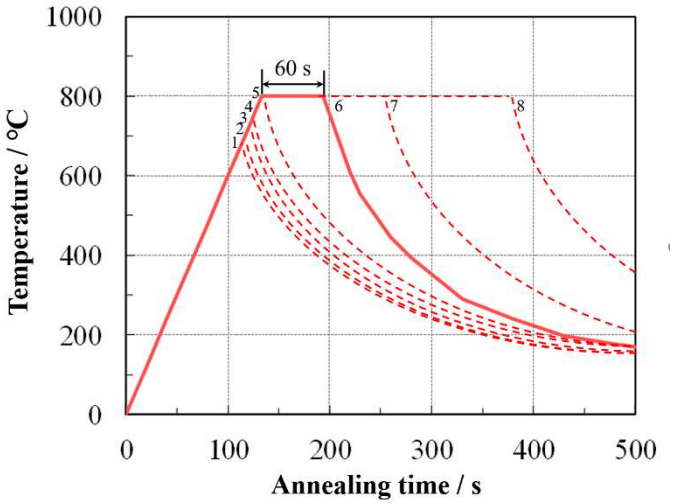

Fig. 1. Temperature profiles of annealing experiments (6: representative profile of industrial continuous annealing; 1-5, 7 and 8: temperature profiles for the study of oxidation kinetics).

3 Results

3.1 Chemical state of Fe-Mn alloy surfaces

3.1.1 Chemical state of non-annealed surfaces

XPS spectra of O 1s, Fe 2p and Mn 2p obtained at the surface of non-annealed alloys (after recrystallization annealing and mirror-polishing) are presented in Fig. 2. The two lines of XPS spectra correspond to an analysis conducted at a depth of 0.93 nm (black line) and 4.65 nm (red line) (eq. Fe) from the sample surface. It should be indicated that carbon is adsorbed on the sample

surface, resulting in a measurement error of chemical composition at the extreme surface, so we begin to study the spectra from the second XPS analysis carried out at a depth of 0.93 nm.

At a depth of 0.93 nm (black lines in Fig. 2), O 1s peak is identified between 529.8 and 530.7 eV corresponding to the binding energy of metal oxides (529.5–530.5 eV) [19,20], two small Fe 2p peaks appear at 709.5–710.9 and 722.7–723.7 eV corresponding to the binding energy of Fe_2O_3 (709.8–710.8 eV) [21,22], and no peaks appear in the Mn 2p spectra. Thus, it can be concluded that only Fe_2O_3 oxides can be detected on the sample surfaces, and that no manganese oxides are formed on the surface of non-annealed samples. At a depth of 4.65 nm (red lines in Fig. 2), two Fe 2p peaks appear at 706.9 and 720.1 eV corresponding to the binding energy of metallic Fe (706.6 eV) [21], and no obvious peaks appear in the O 1s and Mn 2p spectra. Thus, no oxides can be detected at the depth of 4.65 nm. Almost all oxides formed during recrystallization annealing were removed by polishing. The iron oxides analyzed on the very top surface of Fe-Mn alloys (0 to 4.65 nm eq. Fe) are native oxides formed by contact with ambient air. No obvious peaks appear in Mn 2p spectra and its intensity is low due to its low content (1 wt.%) in the alloy.

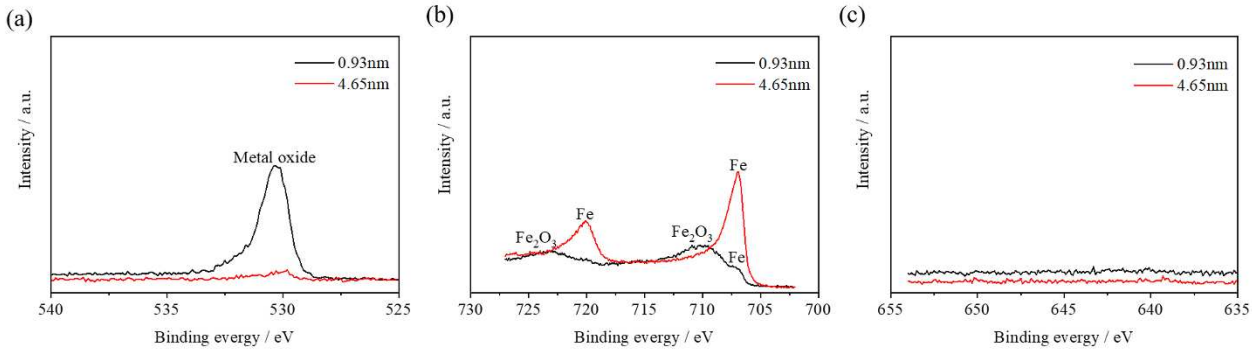

Fig. 2. XPS spectra of (a) O 1s, (b) Fe 2p and (c) Mn 2p obtained at a depth of 0.93 nm (black lines) and 4.65 nm (red lines) (eq. Fe) from the surface of no-annealed samples.

3.1.2 Chemical state of annealed surfaces

Figs. 3 and 4 show the XPS spectra of O 1s, Fe 2p and Mn 2p obtained on the surface of Fe-Mn alloys annealed at 680, 700, 730, 750 and 800 °C during heating and at 800 °C for 60, 120 and 180 s during isothermal holding. At a depth of 0.93 nm (eq. Fe) (Figs. 3(a)-(c) and 4(a)-(c)), the O 1s peaks lie at 530.4 eV and the Fe 2p peaks at 710.4 eV, corresponding to the binding energy of both elements in Fe_2O_3. The maximum intensity of Mn 2p peaks lies between 641.0 and 642.1 eV with a satellite feature at ~647 eV, indicating the presence of only one type of manganese oxide, i.e. MnO [21,23]. It can be seen that Fe peaks always show the same intensity at a depth of 0.93 nm, meaning that iron oxidation remains the same on the alloy surface regardless of the annealing temperature

and time. Mn peak intensity at the depth of 0.93 nm increases as annealing temperature or time increases, meaning that more and more MnO is formed on the alloy surface during annealing treatment. It should be noted that the XPS spectra obtained for Mn and Fe at a depth of 9.3 nm from the sample annealed at 730 ℃ are different from the others (Fig. 3(d)-(f)). The peak intensities of these spectra are lower than at other temperatures. This may be due to a fluctuation in the measurement parameters. Although the spectra intensity is low, the peak of Fe 2p and Mn 2p can be clearly distinguished and the conclusions above remain valid.

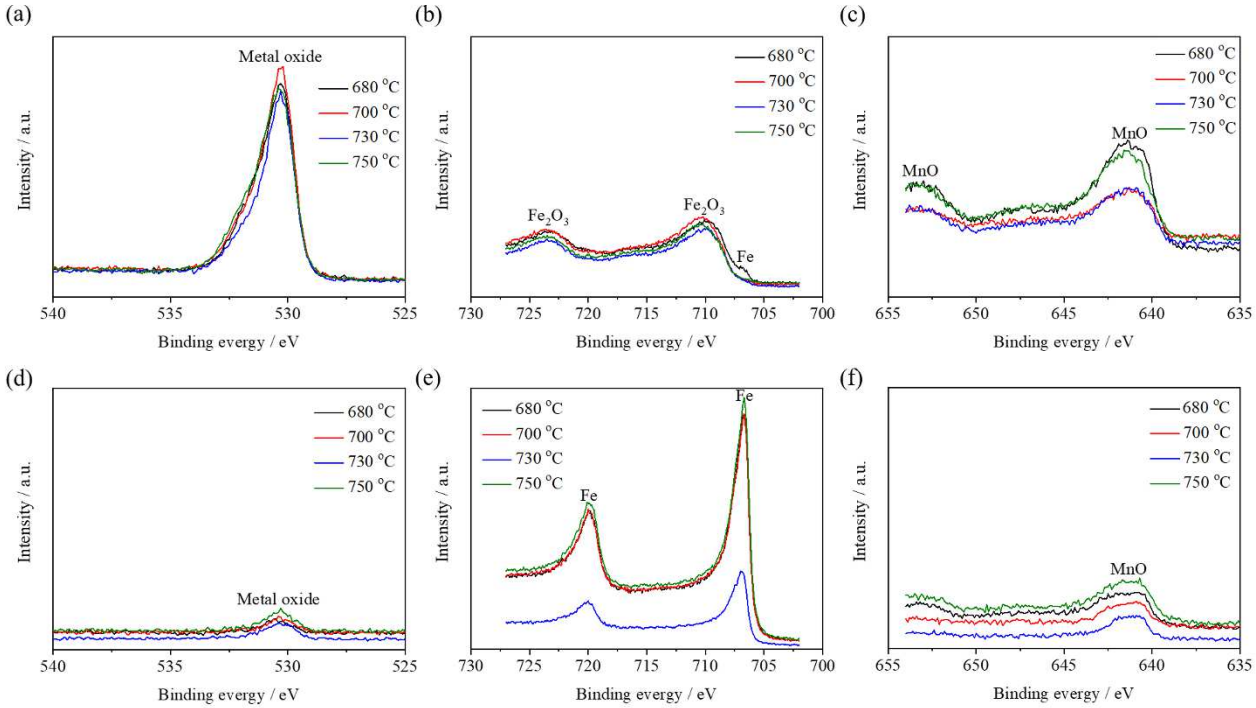

Fig. 3. XPS spectra of (a, d) O 1s, (b, e) Fe 2p and (c, f) Mn 2p obtained at a depth of (a–c) 0.93 nm and (d–f) 9.3 nm (eq. Fe) from the surface of samples annealed at different temperatures during heating.

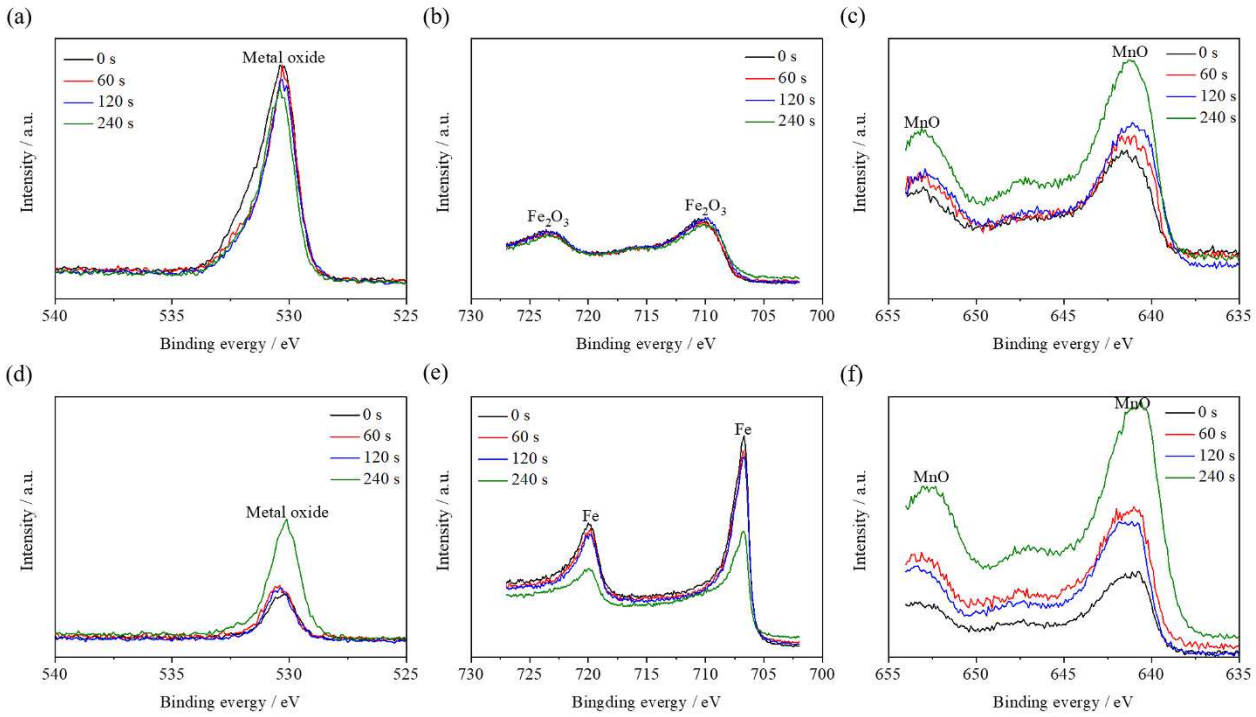

Fig. 4. XPS spectra of (a, d) O 1s, (b, e) Fe 2p and (c, f) Mn 2p obtained at a depth of (a-c) 0.93 nm and (d-f) 9.3 nm (eq. Fe) from the surface of samples annealed at 800 °C for different time during isothermal holding.

At a depth of 9.3 nm (eq. Fe) (Figs. 3(d)–(f) and 4(d) –(f)), the O 1s peaks are at 530.4 eV, the Fe 2p peaks at 706.9 eV and the Mn 2p peaks at 641.0 eV, indicating coexistence of MnO and metallic iron. At annealing temperatures less than or equal to 750 °C (Fig. 3(d) and (f)), the intensity of O and Mn peaks is very low, meaning that MnO oxides are much less present at a depth of 9.3 nm than at the surface (0.93 nm). At a depth of 9.3 nm, as the annealing temperature increases to 800 °C and the annealing time is longer at 800 °C, the intensity of O and Mn peaks increases (Fig. 4(d) and (f)). The intensity of O peak is lower than at the extreme surface because it corresponds to MnO, iron being essentially in metallic form (Fig. 4(e)). The intensity of Mn peak is high (Fig. 4(f)) and remains comparable to that of the surface peak (Fig. 4(c)), which means that the presence of MnO is significant at this erosion depth. The intensity of Mn peak is lower than that measured at the extreme surface for an annealing time at 800 °C of less than 120 s and becomes of the same order of magnitude for an annealing time of 240 s. This indicates that the oxidation depth or the oxide thickness increases with a longer annealing time.

Finally, MnO oxides are present on the surface and below the surface of annealed Fe-Mn alloys. MnO is detected together with metallic iron as the erosion depth increases. The intensity of Mn peaks increases as the annealing temperature or time increases. Native iron oxides analyzed at the

extreme surface are probably formed after annealing in the infrared lamp furnace when the samples are placed in the ambient air.

3.1.3 Changes in Fe chemical state

Fig. 5 shows the changes in Fe chemical state on the surface of samples annealed at 680, 700, 730, 750 and 800 °C during heating and at 800 °C for 60, 120 and 240 s during isothermal holding. At a depth of 0.93 nm (eq. Fe), Fe 2p peaks always lie between 710.2 and 710.6 eV, which correspond to the binding energy of Fe_2O_3. As the depth increases, the peaks of Fe 2p spectra move slightly to the right side of the coordinate axis. The first peak, corresponding to iron oxides, shifts slightly towards the lowest binding energies and is between 709.2 and 710.3 eV (red and blue lines in Fig. 5). The second peak, corresponding to metallic iron, becomes more and more visible at an erosion depth greater than 4 nm (eq. Fe) and lies between 706.7 and 706.9 eV (blue and green lines in Fig. 5). This means that the nature of iron oxides changes as the analysis depth increases and that no iron oxide is present when the depth reaches 4.65 nm at 680 °C, 6.51 nm at 700 °C, 7.44 nm at 730 and 750 °C, 8.37 at 800 °C for 0, 60 and 120 s holding and 9.30 nm at 800 °C for 240 s holding. In summary, iron oxides are present deeper and deeper in the alloy, or their thickness increases as the annealing time increases. The reference binding energies for Fe_2O_3 and FeO peaks are 709.8-710.8 and 708.4-709.5 eV [21,22]. Thus, the iron oxides on the extreme top surface should be Fe_2O_3, and they are FeO or the mixture of Fe_2O_3 and FeO as the depth increases. MnO is also analyzed at the same time for the same depths (Figs. 3(c) and (f), 4(c) and (f)). It can be deduced that MnO could be combined with a small amount of FeO at the alloy surface.

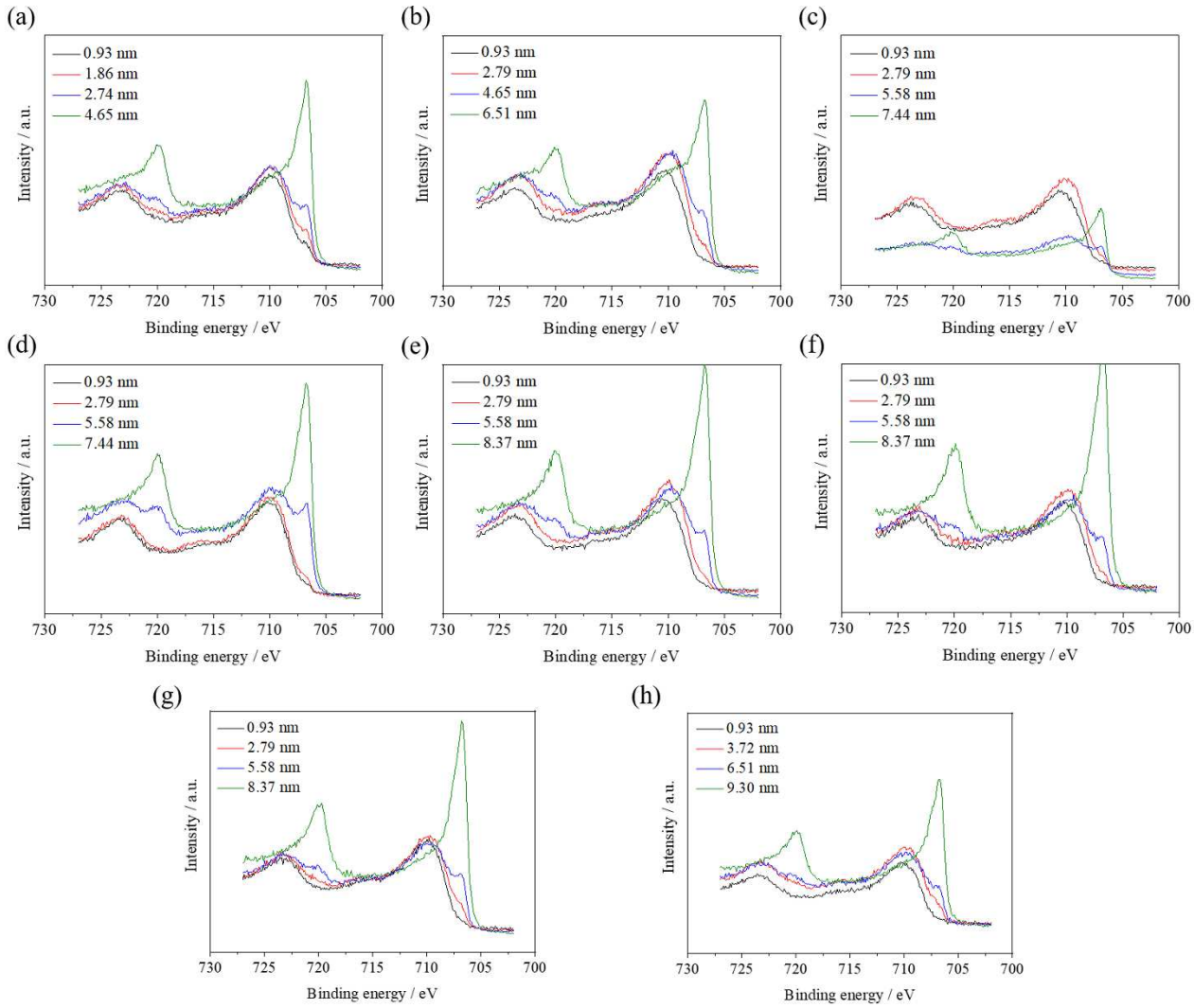

Fig. 5. XPS spectra of Fe 2p obtained on the surface of samples annealed at (a) 680 °C, (b) 700 °C, (c) 730 °C, (d) 750 °C and (e) 800 °C during heating and at 800 °C for (f) 60 s, (g) 120 s and (h) 240 s during isothermal holding (The value of the erosion depth for the different spectra is related to an equivalent depth in pure iron).

3.2 Depth-dependent alloy modification

Fig. 6 shows XPS spectra of Mn 2p obtained at different depths on alloy annealed at 800 °C for 60 s. The peaks of Mn 2p are between 641.0 and 642.0 eV, meaning that all oxide particles formed are MnO oxides. The intensity of Mn 2p peaks decreases gradually from the alloy surface to a depth of 85.3 nm. From a depth of 142.3 nm, no peaks are visible and Mn is no longer oxidized.

Fig. 7 shows STEM images and corresponding EDS maps obtained on the cross-sections of Fe-Mn alloys annealed at 800 °C for 60 s. MnO oxides are mainly formed on the alloy surface. A small amount of oxides are located at a depth of about 80 nm below the surface. Almost no oxides appear in the alloy, but a few areas slightly enriched in O and Mn can also be detected occasionally (bottom of Fig. 7(i) and (l)). Thus, the selective oxidation of Mn is mainly external. The height of

the oxides formed on the alloy surface varies from 20 nm on Fe(110) grains to 40 and 70 nm on Fe(100) and Fe(111) grains respectively. The oxidation depth measured by XPS (here about 80 nm) is of the same order of magnitude as the maximum height of the oxides measured from STEM images.

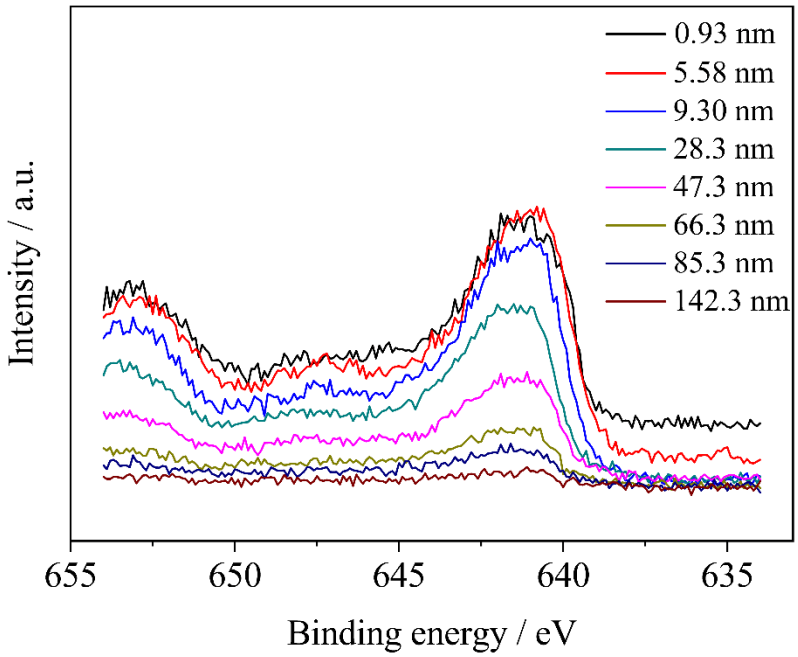

Fig. 6. XPS spectra of Mn 2p obtained on the surface of samples annealed at 800 °C for 60 s (The value of the erosion depth for the different spectra is related to an equivalent depth in pure iron).

The oxidation depth measured by XPS is performed on an average of ten ferrite grains and gives a relatively good estimate of the oxidation measurements. Subsequently, we will look at the behavior of the material as a function of depth based on the XPS measurements. The chemical concentration of the elements detected (Mn, Fe and O) was obtained from the intensity of XPS spectra as well as the relative sensitivity factor of each element.

3.2.1 Oxidation of Mn and Fe

First consider the concentration profiles obtained on the Fe-Mn (1 wt.%) alloy annealed at 800 °C for 60 s (line 6 in Fig. 1), which is representative of industrial annealing. Fig. 8(a) shows the atomic concentration profiles for O, Fe and Mn as a function of depth on the sample annealed at 800 °C for 60 s, abscissa 0 corresponding to the alloy surface. Significant enrichment in Mn at the alloy surface can be observed up to a depth of 100 nm, and a slight enrichment in Mn ranging from 100 nm to approximately 150 nm can also be observed. The depletion of Fe extends from the alloy surface to a depth of 150 nm, correlating well with the enrichment of Mn. In the first tens of nanometers, the Fe

concentration is much less than that of the alloy bulk, due to the formation of MnO oxides at the alloy surface. The O concentration decreases to almost zero at a depth of 150 nm from the alloy surface, corresponding well with Fe depletion and Mn enrichment.

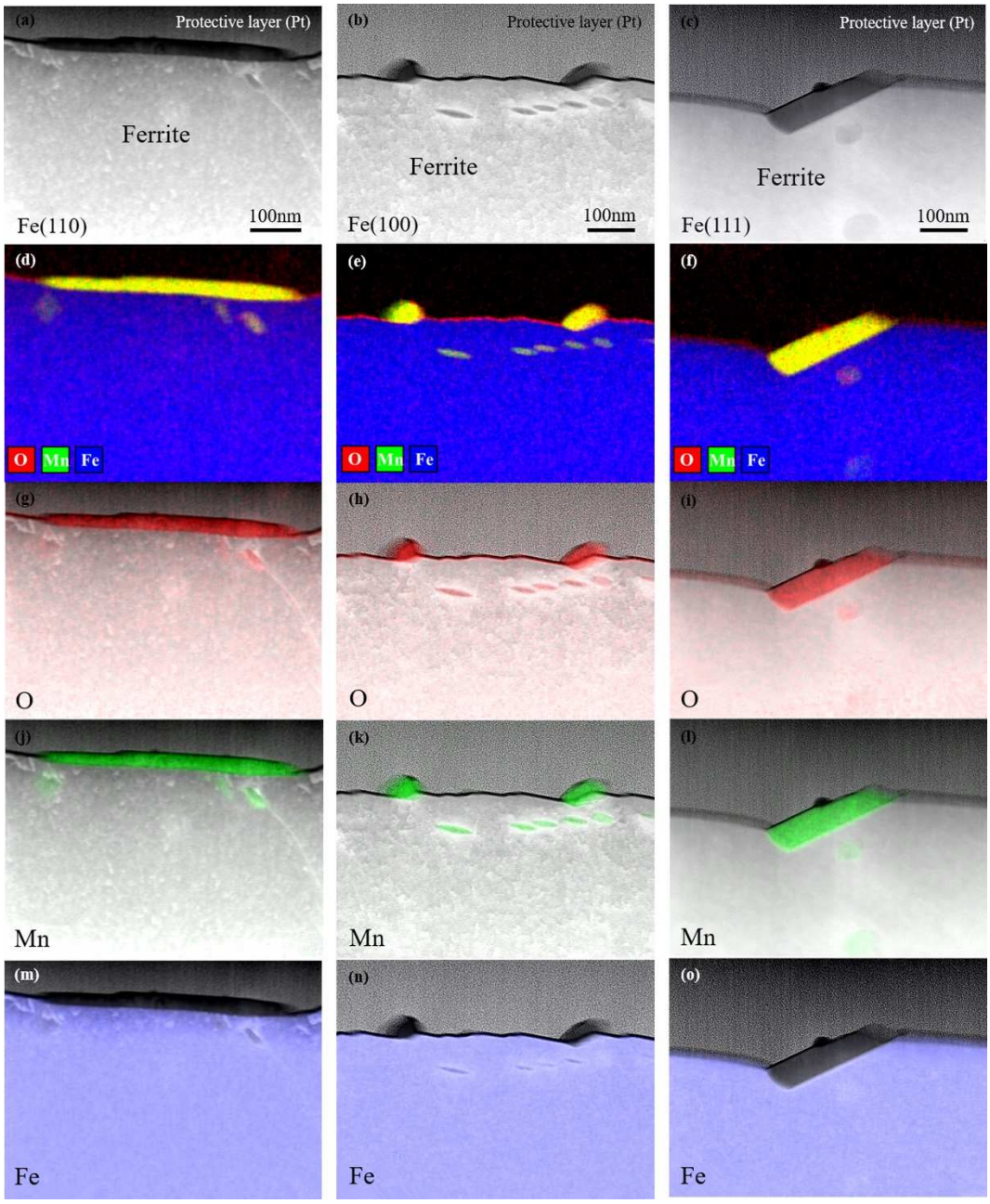

Fig. 7. (a-c) TEM images and EDS mapping of (g)-i) O, (j-l) Mn, (m-o) Fe and (d-f) O-Mn-Fe all together obtained on Fe-Mn alloys annealed at 800 ℃ for 60 s.

Atomic concentration of O is greater than the sum of Mn and Fe in the first 8 nm (red line in Fig. 8(b)), which means that both Mn and Fe oxidize on the alloy surface. At a depth of 0 nm, the O concentration is four times higher than that of Mn and Fe, which means that a lot of oxygen atoms are adsorbed on the alloy surface. In the range from 8 nm to 150 nm, the atomic concentration of O

is approximately equal to that of Mn (black line in Fig. 8(b)), meaning that only Mn is oxidized in this area. The fluctuation of the O/Mn atomic ratio around 1 at a depth of greater than 150 nm is due to the measurement uncertainty. The XPS spectra of Fe on the sample annealed at 800 ℃ for 60 s also show that only metallic Fe can be detected from a depth of about 8 nm (Fig. 5(f)).

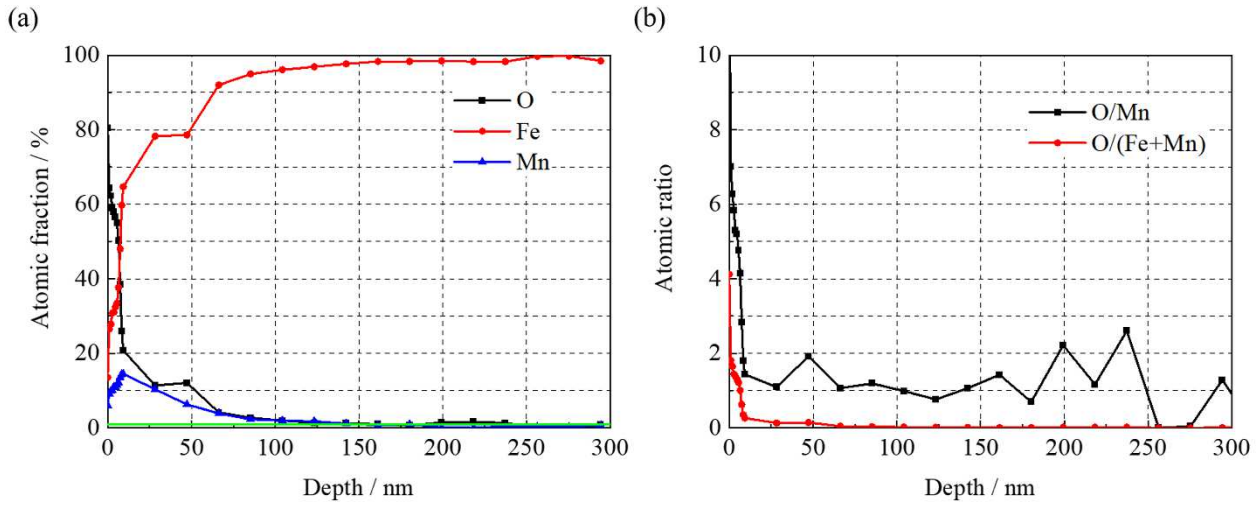

Fig. 8. (a) Atomic fraction for O, Fe and Mn and (b) atomic ratio of O to Mn (black line) and O to Fe+Mn (red line) as a function of depth on the sample annealed at 800 ℃ for 60 s (The green line in Fig. 8(a) represents bulk concentration of Mn (1 wt.% or 1.02 at.%), the depth measurement is based on the assumption that the sputtering rate for Fe is comparable to that of oxidized Fe-Mn (1 wt.%) alloy).

3.2.2 Mn oxidation as a function of annealing time

Fig. 9 shows the evolution of the atomic concentration of Mn as a function of alloy depth for samples annealed at 750 and 800 ℃ during heating and 800 ℃ for holding of 60, 120 and 240 s. All concentration profiles present the same characteristics: Mn concentrations first increase to the peak value at a depth of 8–10 nm and then decrease between 8–10 nm and about 50–300 nm to the bulk composition. These Mn concentration profiles also show some differences during different annealing steps: (1) the maximum value of Mn concentration at a depth of 8–10 nm increases and (2) the Mn enrichment zone in the subsurface extends as the annealing temperature and time increase. The maximum value of Mn concentration corresponds to the maximum amounts of MnO oxides formed on the alloy surface. On the sample annealed at 750 ℃ during heating, the maximum value of Mn concentration is about 6.5 at.%, which means that only a small amount of MnO oxides have been formed on the alloy surface. As the annealing temperature or time increases, increasing

Mn atoms diffuse from the alloy bulk to the surface and participate in the formation and growth of MnO oxides, resulting in a higher peak value of Mn concentration at the alloy surface and a wider range of Mn enrichment in the alloy subsurface.

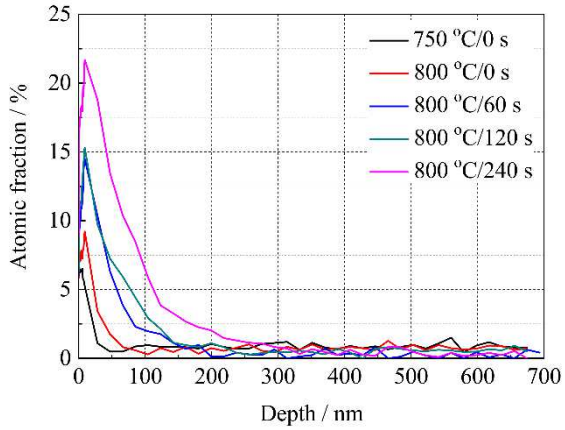

Fig. 9. Concentration profiles (at.%) for Mn as a function of alloy depth obtained on the samples annealed at 750 and 800 °C during heating and at 800 °C for 60, 120 and 240 s-holding (The depth measurement is based on the assumption that the sputtering rate for pure iron is comparable to that of partly oxidized of Fe-Mn (1 wt.%) alloy).

According to the model of selective oxidation [24], an oxidation front with minimal Mn concentration must be present in the alloy subsurface. To show more details of the subsurface concentration profiles, Mn atomic concentration profiles ranging from 0 to 4 at.% are enlarged in Fig. 10. It can be seen that the Mn concentrations decrease to a low concentration point, and then oscillate around 1 at.%. In all cases studied here, the bulk Mn concentration measured by XPS is slightly less than 1 at.% due to a small uncertainty in the calibration of concentration. The XPS measurement uncertainty combined with the low Mn concentration in the studied alloy makes it difficult to precisely locate the oxidation front and to highlight the depletion zone linked to Mn consumption by the formation of MnO. In order to obtain an order of magnitude of the oxidation depth, we have marked the oxidation front with the first measured point at a concentration of less than 0.5 at.% Mn (points in Fig. 10). The depth of the oxidation front increases from 47 nm for annealing at 750 °C to 332 nm for annealing at 800 °C for 240 s. The formation of oxides on the alloy surface consumes Mn in the subsurface regions, resulting in Mn depletion at a low concentration, which corresponds to the equilibrium value of MnO solubility product in iron [25,26].

When the equilibrium concentration of Mn is reached at the oxidation front, the oxidation front goes further and further from the alloy surface for more Mn elements oxidizing.

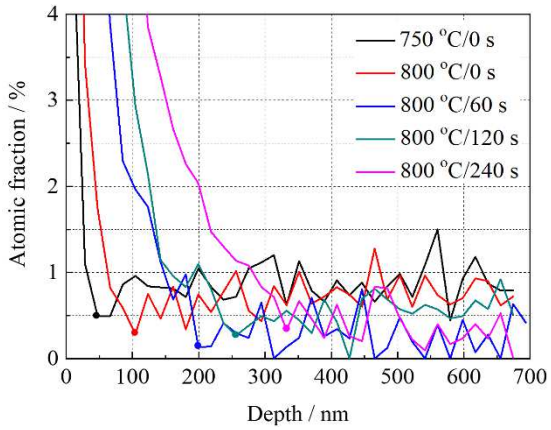

Fig. 10. Concentration profiles (at.%) for Mn as a function of alloy depth for locating the position of the oxidation front (point on the lines) obtained on the samples annealed at 750 and 800 °C during heating and at 800 °C for 60, 120 and 240 s-holding (The depth measurement is based on the assumption that the sputtering rate for pure iron is comparable to that of partly oxidized Fe-Mn (1 wt.%) alloy).

4. Model construction and estimation of Mn diffusion coefficient in ferrite

4.1 Four zones to describe the selective oxidation of the Fe-Mn alloy

XPS results showed that the samples of Fe-Mn alloys annealed in an atmosphere of N_2-5 vol.% H_2 with -40 °C dew point are divided into four zones according to the depth from the alloy surface: an ambient air contaminated zone, a MnO oxide enrichment zone, a Mn depletion zone and the bulk composition zone. In the following, we combined XPS spectra and concentration profiles to analyze the material nature and the boundary conditions of the four zones.

4.1.1 Ambient air contaminated zone

XPS spectra of Fe 2p in Fig. 5 show that iron oxides exist only on the top surface (from the surface to a depth of 4.5–9.0 nm), and that the oxides are more likely to be Fe_2O_3 in the upper part of the iron oxide layer and to be FeO or the mixture of FeO and Fe_2O_3 in the lower part. Fe_2O_3 oxides are also analyzed on the surface of non-annealed samples (about 5 nm thick, Fig. 2), Fe_2O_3 is therefore formed partly or completely on the surface of the annealed samples when the samples are cooled in the N_2-H_2 reducing atmosphere with respect to iron oxides and then released into the

ambient air. The presence of FeO detected on the surface of the annealed alloy can be explained by three main reasons: (1) The formation of FeO-MnO solid solution is thermodynamically possible under the annealing conditions chosen [27]; (2) Oxidation to Fe_3O_4 in the N_2-H_2 reducing atmosphere at low temperature and then to Fe_2O_3 in the ambient air could also lead to the formation of some FeO; (3) The binding energies of FeO and Fe_2O_3 peak are very close and the interpretation could be related to a measurement artifact. Thermodynamic calculations are conducted in Appendix A to validate the possibility of reason (2).

The thickness of the iron oxides on the alloy surface increases slightly with annealing temperature and time: it is 7.4, 8.4, 8.4, 8.4 and 9.3 nm for the samples annealed at 750 and 800 °C during heating and at 800 °C for 60, 120 and 240 s during isothermal holding respectively. This may be due to the increase in oxygen atoms adsorbed on the alloy surface as the annealing temperature and time increase. These adsorbed oxygen atoms participate in the formation of the iron oxide layer at low temperature. The thicknesses of iron oxides coincide with the peak position of Mn concentration profiles shown in Fig. 9. Thus, in the graphs, the air-contaminated zone extends from the alloy surface to the depth where the Mn concentration reaches the maximum. But the difficulty in further interpreting these results is to know how the erosion of the heterogeneous and rough surface composed of MnO particles and iron oxide films takes place. Both materials erode at the same time but are not always in the same plane parallel to the alloy surface.

4.1.2 Enrichment zone of precipitated MnO

XPS spectra and Mn concentration profiles combined with STEM observations show that MnO oxides are formed on the alloy surface with iron oxides in the air-contaminated zone. Then external MnO oxides and a small amount of internal MnO oxides are detected together with metallic iron. In Mn concentration profiles, this area corresponds to the decrease in Mn concentration from the peak position (Fig. 9). To better identify the relationship between the position of the oxidation front and Mn concentration, XPS spectra of Mn 2p obtained at a depth close to oxidation front are presented with Mn concentration in Fig. 11. Peaks corresponding to MnO can be easily observed when the Mn concentration is greater than 3 at.%. The peaks are less visible when the Mn concentration decreases from 3 to 2 at.%. When the Mn concentration is close to 1 at.%, no peaks in the Mn spectra could be observed. Thus, the enrichment zone of precipitated MnO extends from the maximum value to about 1 at.% of the Mn concentration. Fig. 11 also shows the depth where the Mn concentration is between 3 and 1 at.%, i.e., the depth of oxidation front, increases with annealing temperature and time increasing.

Mn concentration reaches a minimum value at the oxidation front (Fig. 10) where thermodynamic equilibrium is reached between Mn and a very small amount of O atoms to fulfill the minimum condition for MnO formation, i.e. the solubility product of MnO in iron:

$$K_{\mathrm{MnO}} = w_{\mathrm{Mn}}^{\mathrm{equi}} \cdot w_{\mathrm{O}}^{\mathrm{equi}} \quad (1)$$

where w_i^{equi} is the concentration of element i in solid iron (in wt.%) at equilibrium with MnO formation. The annealing atmosphere used here is N_2-5 vol.% H_2 with -40 °C dew point, corresponding to a partial pressure of water vapor of 19.05 Pa [28]. The water molecules adsorbed on the alloy surface can dissociate into oxygen atoms dissolved on the sheet. The superficial O concentration in equilibrium with the annealing atmosphere can be expressed as [18]:

$$\lg w_{\mathrm{O}}^{\mathrm{equi}} = 4 - \frac{3690}{T} + \lg \frac{P_{\mathrm{H_2O}}}{P_{\mathrm{H_2}}} \quad (2)$$

where $P_{\mathrm{H_2O}}$ and $P_{\mathrm{H_2}}$ are the partial pressure of water vapor and hydrogen in the atmosphere, and the value of $P_{\mathrm{H_2}}$ is 5066.25 Pa.

With the solubility product of MnO expressed in wt.%^{2} summarized by Huin et al. [18]:

$$K_{\mathrm{MnO}} = 10^{10.95 - \frac{10830}{T}} \times 10^{-8} \quad (3)$$

The equilibrium concentration of Mn for MnO formation in iron is calculated as 0.025 wt.% and 0.053 wt.% at 750 and 800 °C respectively. The measured Mn concentration at the oxidation front larger than the calculated result can be explained by three reasons: (1) The oxidation front we indicated is not the depth limitation where no MnO oxide is formed anymore; (2) The O concentration in equilibrium with the annealing atmosphere is calculated on the alloy surface and the value should be smaller with increased depth; (3) The XPS measurement uncertainty combined with low Mn concentration.

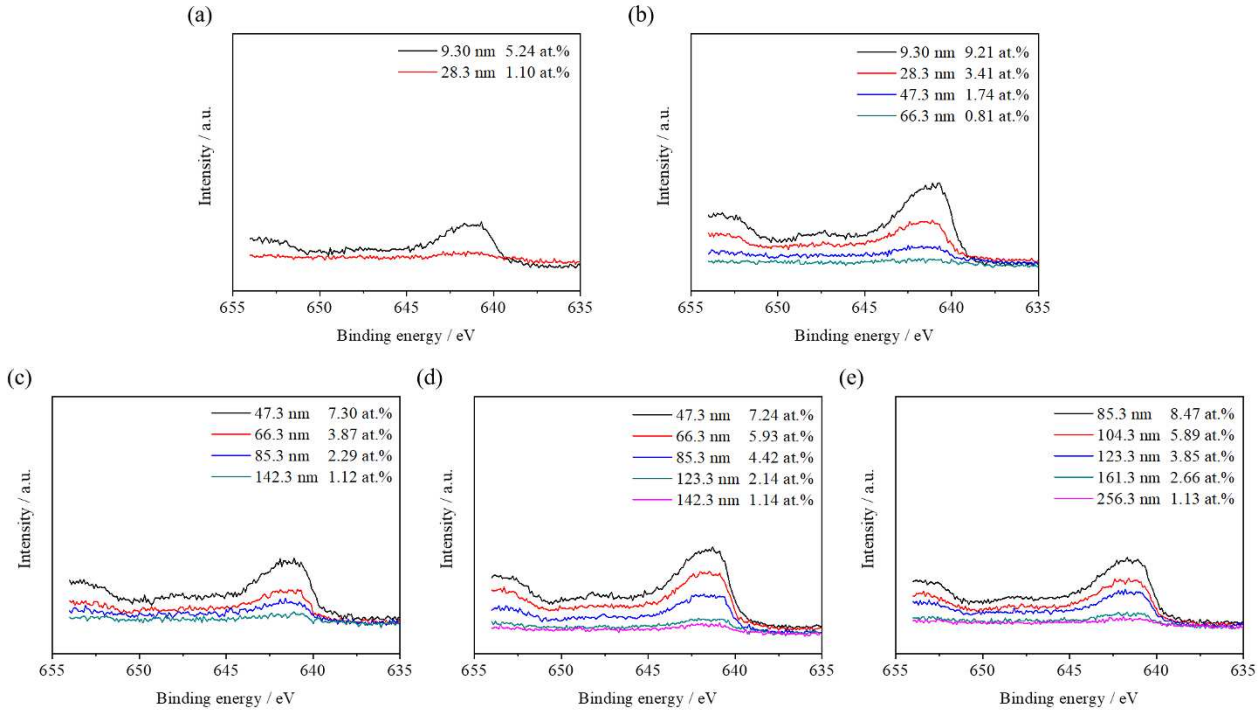

Fig. 11. XPS spectra of Mn 2p obtained on the surface of samples annealed at (a) 750 ℃ and (b) 800 ℃ during heating and at 800 ℃ for (c) 60 s, (d) 120 s and (e) 240 s during isothermal holding (The Mn concentration is given corresponding to different depth, the value of depth for different spectra is assumed to be equivalent to Fe).

4.1.3 Mn depletion zone and bulk composition zone

From the oxidation front, the Mn concentration gradually increases to the bulk composition. This region is the Mn depletion zone. As explained above, the XPS measurement uncertainty combined with low Mn concentration in the studied alloy makes it difficult to precisely locate the oxidation front and to highlight the depletion zone linked to Mn consumption by the formation of MnO. From the measurement of Mn concentration in the bulk, the measurement uncertainty of Mn concentration is about ±0.29 at.%. The five values of Mn concentration (in at.%) at the oxidation front are 0.49, 0.28, 0.13, 0.27 and 0.33. Thus, the measurement uncertainty is comparably large so that cannot be negligible. The boundary between depletion and bulk composition zone cannot be certainly determined from this study.

4.2 Estimation of Mn diffusion coefficient in ferrite

Although the oxidation front and the depletion zone were not precisely located due to measurement uncertainties, we tried to estimate a Mn diffusion coefficient in ferrite using Mn diffusion coefficient.

According to the experimental results, Mn diffuses from the bulk to the oxidation front for the formation of MnO oxides. The diffusion of Mn towards the oxidation front $\xi(t)$ where the Mn concentration reaches its minimum is described by the second Fick's law and the general equation for Mn diffusion as a function of time t and depth x is written as follows:

$$\frac{\partial w_{\mathrm{Mn}}(x,t)}{\partial t} = D_{\mathrm{Mn}} \frac{\partial^2 w_{\mathrm{Mn}}(x,t)}{\partial x^2} \tag{4}$$

where $w_{\mathrm{Mn}}(x,t)$ is the mass fraction of Mn in the alloy and D_{Mn} is the Mn diffusion coefficient in ferrite, assumed here to be independent of temperature and Mn concentration. The use of mass fractions in Eq. (4) instead of the concentrations is valid because the Mn concentration is low (99.0 wt.% Fe) and in that case, it can be assumed that the matrix is well described by pure iron.

The annealing experiments conducted in this work are anisothermal and the heating and cooling time is of the same order of magnitude as the isothermal holding time at 800 °C. The diffusion Eq. (4) to be solved assumes that the temperature is constant and equal to 800 °C. To do this, we will use the experimental results of annealing at 800 °C without holding to estimate an annealing time t_{eq} at 800 °C equivalent to heating and cooling steps from the point of view of Mn diffusion.

Assuming that the annealing is isothermal at 800 °C, thermodynamic equilibrium is reached at the oxidation front $\xi(t)$ between Mn and O for the minimum condition of MnO formation. In this case, the diffusion flux of Mn on the oxidation front $\xi(t)$ is given by:

$$J_{\mathrm{Mn}} = \left(w_{\mathrm{Mn}}^{\mathrm{min}} - w_{\mathrm{Mn}}^{0}\right) \cdot \sqrt{\frac{D_{\mathrm{Mn}}}{\pi \cdot t}} \tag{5}$$

where w_{Mn}^{0} and $w_{\mathrm{Mn}}^{\mathrm{min}}$ are the mass fractions of Mn in the alloy and at the oxidation front $\xi(t)$.

The value of $w_{\mathrm{Mn}}^{\mathrm{min}}$ is equal to the average of Mn mass fraction at the oxidation front obtained on samples annealed at 800 °C for 0, 60, 120 and 240 s and the value is 0.24 ± 0.10 wt.%. The value of w_{Mn}^{0} is equal to 1 wt.% and t used in this equation should be the combination of the equivalent time of heating and cooling steps and the isothermal annealing time, i.e. $t = t_{\mathrm{eq}} + t_{\mathrm{holding}}$.

The total amount of Mn diffusing through the oxidation front $\xi(t)$ within time *t* can be expressed by integrating Eq. (5):

$$m_{\mathrm{Mn}} = 2\left(w_{\mathrm{Mn}}^{0} - w_{\mathrm{Mn}}^{\min}\right) \cdot \sqrt{\frac{D_{\mathrm{Mn}}(t_{\mathrm{holding}} + t_{\mathrm{eq}})}{\pi}} \quad (6)$$

The equivalent time t_{eq} is determined using the measured amount of Mn from the concentration profiles, i.e. the Mn content present from the alloy surface to the oxidation front. The measured amount of Mn is 98.3, 496.4, 583.1 and 1023.3 wt.% nm for samples annealed at 800 °C for 0, 60, 120 and 240 s. Thus t_{eq} is estimated to be 36 s and the evolution of the amount of Mn diffusing through the oxidation front as a function of the square root of $t_{\mathrm{holding}} + t_{\mathrm{eq}}$ is shown in Fig. 12.

With the slop of the straight line in Fig. 12 and Eq. (6), it can be estimated that the value of D_{Mn} is about 2.9×10^{-15} m^2 s^{-1} at 800 °C. In literature, values for D_{Mn} at 800 °C is equal to 9.09×10^{-16} m^2 s^{-1} according to Oikawa [29], 7.0×10^{-16} m^2 s^{-1} according to Kucera et al. [30] and 2.6×10^{-15} m^2 s^{-1} according to Ollivier-Leduc et al [1]. Our calculation results are a little larger than the published values for three reasons: (1) We assumed the location of the first point in Mn concentration profiles lower than 0.5 at.% corresponding to the oxidation front. The real oxidation front is probable in deeper alloy due to large measurement uncertainty. (2) The depth measurement in Mn concentration profiles is based on the assumption that the sputtering rate for pure iron is comparable to that of Fe-Mn (1 wt.%) alloy, which may lead to an overestimate of depth and thus larger m_{Mn} in Eq. (6). (3) The diffusion coefficient estimated in this work is a combination of bulk and grain boundary diffusion.

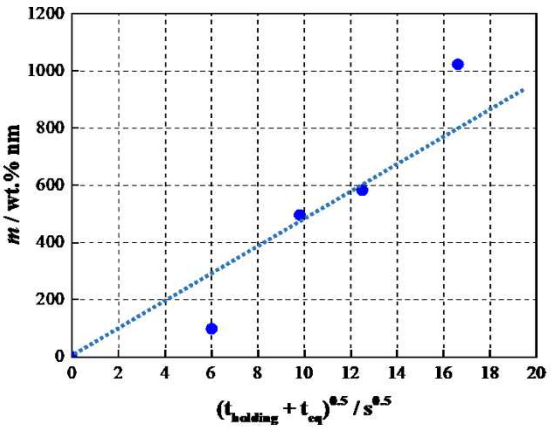

Fig. 12. Evolution of the amount of Mn diffusing through the oxidation front as a function of the square root of $t_{\mathrm{holding}} + t_{\mathrm{eq}}$ at 800 °C.

5. Conclusions

Selective oxidation of Fe-Mn alloys was studied by XPS during annealing treatments conducted in industrial continuous annealing conditions to explore the nature of oxides formed in different depths from alloy surface and the characteristics of selective oxidation of Fe-Mn alloys during annealing. Under the industrial annealing conditions, only MnO oxides are formed on and below the surface and few iron oxides appear on the very top surface due to oxidation of ambient air or the formation of FeO-MnO solid solutions. The concentration profiles obtained are typical mode of selective oxidation: diffusion of Mn from the alloy bulk to the oxidation front and selective oxidation on the alloy surface. From XPS spectra and Mn concentration profiles as a function of depth, the samples annealed in N_2-H_2 atmosphere are divided into four zones: ambient air contaminated zone (a few nanometers thick on the surface), MnO oxide enrichment zone (from the maximum value to about 1 at.% of Mn concentration), Mn depletion zone and bulk composition zone (unclear boundary because of measurement uncertainty). In the MnO enrichment zone, XPS signal of MnO is intense at first and then decreases rapidly until the Mn concentration is about 3 at.%, corresponding to the external and internal oxidation zone. No peaks in Mn spectra could be observed when the Mn concentration is close to 1 at.%. The Mn concentration reaches a minimum value at the oxidation front, whose position is deeper with annealing temperature and time increasing. The value of Mn diffusion coefficient in ferrite estimated using diffusion flux at the oxidation front is 2.9×10^{-15} m^2 s^{-1} at 800 °C, which is a slightly larger than that in literature.

Appendix A: Thermodynamic calculations

A.1 Thermodynamic stability of Fe_3O_4 in N_2-5 vol.% H_2 atmosphere

The reactions between iron (Fe) and its oxides (Fe_xO_z) in the annealing atmosphere of N_2-5 vol.% H_2 are given by:

$$x\,\mathrm{Fe(s)} + z\,\mathrm{H_2O(g)} \leftrightarrow \mathrm{Fe_xO_z(s)} + z\,\mathrm{H_2(g)} \qquad \text{(R-A.1)}$$

The Gibbs free energy associated with reaction (R-A.1) under constant temperature and pressure can be expressed as [34]:

$$\Delta_r G_{\mathrm{R-A.1}} = \Delta_r G^{\circ}_{\mathrm{R-A.1}} + RT \ln\left(\frac{a_{\mathrm{Fe_xO_z}}}{a_{\mathrm{Fe}}^{x}} \frac{{P_{\mathrm{H_2}}}^{z}}{{P_{\mathrm{H_2O}}}^{z}}\right) \qquad \text{(A.1)}$$

where $\Delta_r G^{\circ}_{\mathrm{R-A.1}}$ is the standard Gibbs free energy of reaction (R-A.1), and $a_{\mathrm{Fe_xO_z}}$ and a_{Fe} are the activities of Fe_xO_z and Fe. As a first approximation, the oxides formed can be considered to be pure, i.e., $a_{\mathrm{Fe_xO_z}} = 1$. As Fe is the main element in Fe-Mn alloy studied there (99.00 wt.%), its activity is supposed to be given by Raoult's law:

$$a_{\mathrm{Fe}} = x_{\mathrm{Fe}} \approx 1 \qquad \text{(A.2)}$$

The value of $\Delta_r G^{\circ}_{\mathrm{R-A.1}}$ can be taken from FactSage 7.2 (http://www.factsage.com/), and the values of $P_{\mathrm{H_2}}$ and $P_{\mathrm{H_2o}}$ in the annealing atmosphere used in this work are 5066.25 and 19.05 Pa respectively.

With all the equations and values given above, the thermodynamic stability of iron oxides, i.e. $Fe_{0.95}O$, Fe_2O_3 and Fe_3O_4 can be determined as a function of annealing temperature. It is found that only Fe_3O_4 is thermodynamic stable in N_2-5 vol.% H_2 atmosphere in the temperature range of 0 °C to 175 °C. Thus, Fe_3O_4 can be formed when the samples are cooled in the N_2-H_2 reducing atmosphere after annealing treatment.

A.2 Thermodynamic stability of Fe_2O_3 in ambient air

The reactions between iron and Fe_2O_3 in the ambient air are given by:

$$2\,\mathrm{Fe(s)} + \frac{3}{2}\,\mathrm{O_2(g)} \leftrightarrow \mathrm{Fe_2O_3(s)} \qquad \text{(R-A.2)}$$

The Gibbs free energy associated with reaction (R-A.2) under constant temperature and pressure can be expressed as [31]:

$$\Delta_r G_{\mathrm{R-A.2}} = \Delta_r G^{\circ}_{\mathrm{R-A.2}} + RT \ln\left(\frac{a_{\mathrm{Fe_2O_3}}}{a^2_{\mathrm{Fe}}}\frac{1}{{P_{\mathrm{O_2}}}^{3/2}}\right) \quad \text{(A.3)}$$

where $\Delta_r G^{\circ}_{\mathrm{R-A.2}}$ is the standard Gibbs free energy of reaction (R-A.2), and $P_{\mathrm{O_2}}$ is the oxygen partial pressure in ambient air, whose value is 21278.25 Pa. Since the activities of Fe_2O_3 and Fe are equal to 1, Fe_2O_3 can be stable in ambient air when:

$$\Delta_r G^{\circ}_{\mathrm{R-A.2}} - \frac{3}{2} RT \ln P_{\mathrm{O_2}} < 0 \quad \text{(A.4)}$$

The value of $\Delta_r G^{\circ}_{\mathrm{R-A.2}}$ (from FactSage 7.2) at room temperature (22 ℃) is -825821.3 J, so Fe_2O_3 can stably exit in the ambient air.

A.3 Transformation of Fe_3O_4 into Fe_2O_3 and Fe_2O_3+FeO in ambient air

The Gibbs free energy of transformation of Fe_3O_4 into Fe_2O_3 can be calculated using Eq. (A.5).

$$4\,\mathrm{Fe_3O_4(s)} + \mathrm{O_2(g)} = 6\,\mathrm{Fe_2O_3(s)} \quad \text{(R-A.3)}$$

$$\Delta_r G_{\mathrm{R-A.3}} = \Delta_r G^{\circ}_{\mathrm{R-A.3}} + RT \ln \frac{a^6_{\mathrm{Fe_2O_3}}}{a^4_{\mathrm{Fe_3O_4}} \cdot P_{\mathrm{O_2}}} \quad \text{(A.5)}$$

where $\Delta_r G^{\circ}_{\mathrm{R-A.3}}$ is the standard Gibbs free energy of reaction (R-A.3), and its value is -485102.5 J at 22 ℃ (from FactSage 7.2). Thus, the Gibbs free energy of transformation of Fe_3O_4 into Fe_2O_3 is much less than zero in ambient air at room temperature.

The Gibbs free energy of transformation of Fe_3O_4 into Fe_2O_3+FeO can be calculated using Eq. (A.6).

$$5\,\mathrm{Fe_3O_4(s)} + \mathrm{O_2(g)} = 7\,\mathrm{Fe_2O_3(s)} + \mathrm{FeO(s)} \quad \text{(R-A.4)}$$

$$\Delta_r G_{\mathrm{R-A.4}} = \Delta_r G^{\circ}_{\mathrm{R-A.4}} + RT \ln \frac{a^7_{\mathrm{Fe_2O_3}} \cdot \mathrm{FeO}}{a^5_{\mathrm{Fe_3O_4}} \cdot P_{\mathrm{O_2}}} \quad \text{(A.6)}$$

where $\Delta_r G^{\circ}_{\mathrm{R-A.4}}$ is the standard Gibbs free energy of reaction (R-A.4), and its value is -459329.4 J at 22 ℃ (from FactSage 7.2). Since the Gibbs free energy of transformation of Fe_3O_4 into Fe_2O_3+FeO is much less than zero at room temperature, it is possible that some FeO is formed when Fe_3O_4 is transformed into Fe_2O_3 in ambient air.

Declaration of competing interest:

The authors declare that they have no known competing financial interests or personal relationships that could have appeared to influence the work reported in this paper.

Acknowledgements

This work was financially supported by the French "Agence Nationale de la Recherche" through the "Investissements d'avenir" Program (No. ANR-10-EQPX-37 MATMECA) and the Chinese "International Exchange Program" (No. YJ20210129). The authors thank the Shuimu Tsinghua Scholar Program (No. 2020SM100).

References

[1] A. Ollivier-Leduc, M.-L. Giorgi, D. Balloy, J.-B. Guillot, Study of selective oxidation by means of glow discharge optical emission spectroscopy, Corros. Sci. 53 (2011) 1375-1382.

[2] V.F.C. Lins, L. Madeira, J.M.C. Vilela, M.S. Andrade, V.T.L. Buono, J.P. Guimaraes, E.A. Alvarenga, Selective oxidation of dual phase steel after annealing at different dew points, Appl. Surf. Sci. 257 (2011) 5871-5878.

[3] G. Wu, J. Zhang, Effect of water pressure and soaking time on the selective oxidation of DP980 advanced high strength steel, Appl. Surf. Sci. 453 (2018) 252-262.

[4] L. Liu, G. Jiang, H. Wang, H. Teng, Effect of dew point during heating on selective oxidation of TRIP steels, Metall. Res. Technol. 114 (2017) 609-614.

[5] S.H. Ham, C. Carteret, J. Angulo, G. Fricout, Relation between emissivity evolution during annealing and selective oxidation of TRIP steel, Corros. Sci. 132 (2018) 185-193.

[6] M. Auinger, E.-M. Mueller-Lorenz, M. Rohwerder, Modelling and experiment of selective oxidation and nitridation of binary model alloys at 700 ºC -- The systems Fe, 1 wt.%{Al, Cr, Mn, Si}, Corros. Sci. 90 (2015) 503-510.

[7] A. Ollivier-Leduc, M.-L. Giorgi, D. Balloy, J.-B. Guillot, Nucleation and growth of selective oxide particles on steel, Corros. Sci. 52 (2010) 2498-2504.

[8] H. Wang, X. Jin, G. Hu, Y. He, Changing oxide layer structures with respect to the dew point prior to hot-dip galvanizing of δ-TRIP steel, Surf. Coat. Technol. 337 (2018) 260-269.

[9] M. Pourmajidian, J.R. Mcdermid, Selective oxidation of a 0.1C-6Mn-2Si third generation advanced high-strength steel during dew-point controlled annealing, Metall. Mater. Trans. A 49 (2018) 1795-1808.

[10] K.-K. Wang, C.-W. Hsu, L. Chang, D. Gan, T.-R. Chen, K.-C. Yang, Study of selective oxidation behavior of a 1.2Si-1.5Mn TRIP steel during intercritical annealing, J. Electrochem. Soc. 159 (2012) C561-C570.

[11] L. Cho, C.S. Jung, B.C. De Cooman, On the transition of internal to external elective oxidation on CMnSi TRIP steel, Metall. Mater. Trans. A 45 (2014) 5158-5172.

[12] M. Norden, M. Blumenau, T. Wuttke, K.-J. Peters, The change of steel surface chemistry regarding oxygen partial pressure and dew point, Appl. Surf. Sci. 271 (2013) 19-31.

[13] S.-K. Lee, J.-S. Kim, N. Kang, K.-M. Cho, Effects of furnace atmosphere on selective oxidation behaviour of Si-added transformation-induced plasticity steels, Met. Mater. Int. 18 (2012) 951-956.

[14] K. Shinoda, T. Yamamoto, S. Suzuki, Characterization of selective oxidation of manganese in surface layers of Fe-Mn alloys by different analytical methods, ISIJ Int. 53 (2013) 2000-2006.

[15] I. Cvijovic, I. Parezanovic, M. Spiegel, Influence of N_2-H_2 atmosphere composition and annealing duration on the selective surface oxidation of low-carbon steels, Corros. Sci. 48 (2006) 980-993.

[16] L. Gong, N. Ruscassier, M. Ayouz, P. Haghi-Ashtiani, M.-L. Giorgi, Analytical model of selective external oxidation of Fe-Mn binary alloys during isothermal annealing treatment, Corros. Sci. 166 (2020) 108454.

[17] L. Gong, N. Ruscassier, P. Chrétien, P. Haghi-Ashtiani, L. Yedra, M.-L. Giorgi, Nucleation and growth of oxide particles on a binary Fe-Mn (1 wt.%) alloy during annealing, Corros. Sci. 177 (2020) 108952.

[18] D. Huin, P. Flauder, J.-B. Leblond, Numerical simulation of internal oxidation of steels during annealing treatments, Oxid. Met. 64 (2005) 131-167.

[19] T. Fujii, F.M.F. de Groot, G.A. Sawatzky, *In situ* XPS analysis of various iron oxide films grown by NO_2-assisted molecular-beam epitaxy, Phys. Rev. B 59 (1999) 3195-3202.

[20] J.-C. Dupin, D. Gonbeau, P. Vinatier, A. Levasseur, Systematic XPS studies of metal oxides, hydroxides and peroxides, Phys. Chem. Chem. Phys. 2 (2000) 1319-1324.

[21] M.C. Biesinger, B.P. Payne, A.P. Grosvenor, L.W.M. Lau, A.R. Gerson, R. St.C. Smart, Resolving surface chemical states in XPS analysis of first row transition metals, oxides and hydroxides: Cr, Mn, Fe, Co and Ni, Appl. Surf. Sci. 257 (2011) 2717-2730.

[22] A.P. Grosvenor, B.A. Kobe, M.C. Biesinger, N.S. Mclntyre, Investigation of multiplet splitting of Fe 2p XPS spectra and bonding in iron compounds, Surf. Interface Anal. 36 (2004) 1564-1574.

[23] E.S. Ilton, J.E. Post, P.J. Heaney, F.T. Ling, S.N. Kerisit, XPS determination of Mn oxidation states in Mn (hydr)oxides, Appl. Surf. Sci. 366 (2016) 475-785.

[24] C. Wagner, Reaktionstypen bei der oxydation von legierungen, Zeitschrift fur Elcktrochemie 63 (1959) 772-782.

[25] J.S. Kirkaldy, On the theory of internal oxidation and sulphation of alloys, Can. Metall. Quart. 8 (1969) 35-38.

[26] G.R. Laflamme, J.E. Morral, Limiting cases of subscale formation, Acta Metall. 26 (1978) 1791-1794.

[27] P. Wu, G. Eriksson, A.D. Pelton, Critical evaluation and optimization of the thermodynamic properties and phase diagrams of the CaO-FeO, CaO-MnO, FeO-MgO, FeO-MnO, and MgO-MnO systems, J. Am. Ceram. Soc. 76 (1993) 2065-2075.

[28] D. Sonntag, Important values of the physical constants of 1986, vapor pressure formations based on the ITS-90, and psychrometer formulae, Z. Meteorol 70 (1990) 340-344.

[29] H. Oikawa, Lattice diffusion in iron – A review, ISIJ Int. 68 (1982) 1489-1497.

[30] J. Kucera, K. Stransky, Diffusion in iron, iron solid solutions and steels, Mater. Sci. Eng. 52 (1982) 1-38.

[31] J.P. Novak, S. Labik, I. Malijevska, Chemical Equilibrium, in: J.P. Novak, S. Labik, I. Malijevska (Eds.), Physical Chemistry in Brief, Institute of Chemical Technology, Prague, 2005, pp. 226-261.